Ocean Systems Engineering, Vol. 1, No. 4 (2011) 355-372
DOI: http://dx.doi.org/10.12989/ose.2011.1.4.355

Numerical simulation of fully nonlinear sloshing waves in three-dimensional tank under random excitation

Gang Xu*[1,3], A.M.S. Hamouda[1] and B.C. Khoo[2]

[1]*Department of Mechanical and Industrial Engineering, Qatar University, Qatar*
[2]*Department of Mechanical Engineering, National University of Singapore, Singapore*
[3]*School of Naval Architecture and Ocean Engineering, Jiangsu University of Science and Technology, China*

(Received October 2, 2011, Revised December 2, 2011, Accepted December 12, 2011)

Abstract. Based on the fully nonlinear velocity potential theory, the liquid sloshing in a three dimensional tank under random excitation is studied. The governing Laplace equation with fully nonlinear boundary conditions on the moving free surface is solved using the indirect desingularized boundary integral equation method (DBIEM). The fourth-order predictor-corrector Adams-Bashforth-Moulton scheme (ABM4) and mixed Eulerian-Lagrangian (MEL) method are used for the time-stepping integration of the free surface boundary conditions. A smoothing scheme, B-spline curve, is applied to both the longitudinal and transverse directions of the tank to eliminate the possible saw-tooth instabilities. When the tank is undergoing one dimensional regular motion of small amplitude, the calculated results are found to be in very good agreement with linear analytical solution. In the simulation, the normal standing waves, travelling waves and bores are observed. The extensive calculation has been made for the tank undergoing specified random oscillation. The nonlinear effect of random sloshing wave is studied and the effect of peak frequency used for the generation of random oscillation is investigated. It is found that, even as the peak value of spectrum for oscillation becomes smaller, the maximum wave elevation on the side wall becomes bigger when the peak frequency is closer to the natural frequency.

Keywords: sloshing waves; random waves; desingularized BIEM; fully nonlinearity.

1. Introduction

Sloshing motions of liquid are associated with various engineering problems, such as liquid cargo in a LNG carrier, the liquid oscillations in large storage tanks caused by earthquakes, the motions of liquid fuel in aircraft and spacecraft, the liquid motions in containers and the water flow on the decks of ships. As the motion can become large or even violent when resonance occurs, the liquid load can cause structural damage on the container and/or lead to loss of stability of the liquid carrier such as a ship.

Since sloshing has important implications in engineering, it has been extensively studied over the past years. Abramson (1996) used a linear theory to simulate small amplitude sloshing in a container, Solaas and Faltinsen (1997) employed a perturbation theory. Wu (2007) considered the second-order resonance conditions in a rectangular tank. Firouz Abadi *et al*. (2011) used BEM model to investigate second-order analysis of sloshing in tanks with arbitrary shapes under both

*Corresponding author, Post-doctoral researcher, E-mail: g.xu@qu.edu.qa

horizontal and vertical excitations. For large amplitude sloshing, Faltinsen (1978) adopted the boundary element method to simulate fluid motion in a 2D rectangular container subjected to a horizontal excitation. Cho and Lee (2004) presented a non-linear finite element method for the simulation of large amplitude sloshing in a rectangular baffled tank, subject to horizontal forced excitation. They performed parameter studies on the effects of the baffle on the non-linear liquid sloshing. Chen and Nokes (2005) applied Navier-Stokes equations to study 2D sloshing motion (surge, heave and pitch) in a tank via coordinate transformation. Wu *et al*. (1998) used the finite element method (FEM) and analyzed 3D sloshing waves through the fully nonlinear velocity potential theory. Liu and Lin (2008) used the spatially averaged Navier-Stokes equations to study 3D nonlinear liquid sloshing. Frandsen (2004) conducted a series of numerical experiment in a 2D tank which is moved both horizontally and vertically via *ó*-coordinate transformation. Wu and Chen (2009) used 3D finite difference method to solve for wave sloshing in a 3D tank excited by coupled surge and sway motions. For random sloshing, Wang and Khoo (2005) adopted FEM and considered the 2D nonlinear sloshing problem in a tank under random excitation. Sriram *et al*. (2006) performed the finite element analysis of non-linear sloshing in a rectangular tank under both horizontal and vertical random excitations.

In the present study, the desingularized boundary integral equation method (DBIEM) is selected for simulating 3D random sloshing wave. The method has been successfully used previously in solving nonlinear water wave problems, such as in the work by Beck (1994), Kim *et al*. (1998), Celebi (2001), Kara *et al*. (2007) and Zhang *et al*. (2010). The main advantage of DBIEM, compared with FEM, lies in having only to discretize the surface of fluid domain. When the boundary of the fluid domain is confined and the number of the discretized elements is limited, the DBIEM may offer a better computational efficiency and less memory requirement, even its matrix is fully populated. Compared with the conventional BEM, The integral kernels of the DBIEM are no longer singular as the singularities are placed slightly outside the fluid domain. This is particularly advantageous when the direct differentiation is applied to the integral equation to obtain the velocity.

In this study, we shall focus on the 3D sloshing problem in a rectangular tank. Similar problems have been considered by Wu *et al*. (1998) and Kara *et al*. (2007). Here the DBIEM is employed to solve the boundary value problem at each time step. The fourth-order predictor-corrector ABM4 scheme and mixed Eulerian-Lagrangian (MEL) method are used for the time-stepping integration of the free surface boundary conditions. Since wave breaking is not considered in this work, the position of the nodes on free surface is tracked by applying semi-Lagrangian approach (Zhang *et al*. 2006, Zhang *et al*. 2007, Khoo and Kim 2007), in which the nodes on free surface are allowed to move only in vertical direction, with the horizontal motion of the nodes on the free surface held fixed. This approach has the advantage of avoiding the task of re-gridding the free surface at each time step. For stable time-step simulation a B-spline smoothing scheme is applied in both longitudinal and transverse directions of the tank to prevent saw-tooth instability, and the smoothing scheme is used at every three time steps. Numerical results obtained show that the present desingularized model effective in the simulation for 3D sloshing waves even for the tank under specified random motions.

2. Mathematical formulation

A Cartesian co-ordinate system *oxyz* is defined for 3D sloshing waves. The origin is at the centre

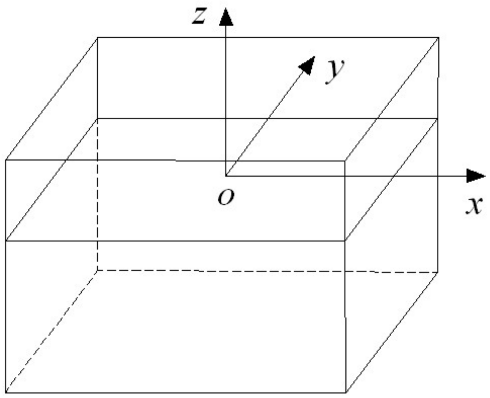

Fig. 1. The co-ordinate system and the sloshing tank

of the undisturbed free surface, as shown in Fig. 1. x and y in the longitudinal and transverse directions of the rectangular tank, z points vertically upwards.

Based on potential flow theory, the velocity potential ϕ in computational fluid domain D satisfies the Laplace equation.

$$\nabla^2\phi = 0 \qquad \text{in}D. \tag{1}$$

We consider only the translational motion of the tank. On the rigid surfaces (Γ_W) of the side wall and the bottom of the tank, the boundary condition on the potential can be written as

$$\frac{\partial\phi}{\partial n} = \boldsymbol{U}\cdot\boldsymbol{n} \qquad \text{on}\Gamma_W \tag{2}$$

where $\boldsymbol{U}$ is the velocity of the tank and $\boldsymbol{n}$ is outward normal vector of the surfaces of the tank wall and bottom.

On the instantaneous free surface Γ_F, the dynamic and kinematic conditions can be written as

$$\frac{\partial\phi}{\partial t} = \frac{1}{2}\nabla\phi\nabla\phi + g\eta \qquad \text{on}\Gamma_F \tag{3}$$

$$\frac{\partial\eta}{\partial t} + \frac{\partial\phi}{\partial x}\frac{\partial\eta}{\partial tx} + \frac{\partial\phi}{\partial y}\frac{\partial\eta}{\partial y} + \frac{\partial\phi}{\partial z} = 0 \qquad \text{on}\Gamma_F \tag{4}$$

where t and g denote time and gravitational acceleration, respectively. The initial conditions may be expressed as

$$\phi(x, y, z = \xi,\ t = 0) = \phi_0(x, y, z) \tag{5}$$

$$\eta(x, y, t = 0) = \xi(x, y) \tag{6}$$

3. Desingularized boundary integral equation method

In this study, the indirect DBIEM is employed to solve the boundary value problem for the

unknown velocity potential $\phi(x,y,z,t)$ at each time step. This method obtains the solution by distributing Rankine sources over a surface S outside the fluid domain D. This surface is at a small distance away from the corresponding real boundary of the fluid. The velocity potential in the fluid domain D can be written as follows

$$\phi(p,t) = \iint_S \sigma(q,t)\frac{1}{r_{pq}}ds_q \tag{7}$$

where $q(\xi,\eta,\zeta)$ is the integration point on the integration surface S outside the fluid domain, $p(x,y,z)$ is the field point where the potential is evaluated, σ is the unknown source strength distribution over the surface S and

$$r_{pq} = \sqrt{(x-\xi)^2+(y-\eta)^2+(z-\zeta)^2} \tag{8}$$

For the problem considered in this work, we construct the solution using a constant-strength source point within each element over the integration boundary S_F and a constant-strength source point over the integration surface S_W, where S_F is the integration surface above the free surface Γ_F, and S_W is the integration surface outside the real boundary Γ_W of the tank. That is

$$\phi(p,t) = \iint_{S_F} \sigma_F(q,t)\frac{1}{r_{pq}}ds_q + \iint_{S_F} \sigma_W(q,t)\frac{1}{r_{pq}}ds_q. \tag{9}$$

By applying the boundary conditions, we obtain boundary integral equations for the unknown strength of the singularities, $\sigma_F(q,t)$ and $\sigma_W(q,t)$, respectively:

$$\iint_S \sigma_F(q,t)\frac{1}{r_{pq}}ds_q + \iint_{S_F} \sigma_W(q,t)\frac{1}{r_{pq}}ds_q = \phi_0(p,t) \qquad (p \in \Gamma_F) \tag{10}$$

$$\iint_{S_F} \sigma_F(q,t)\frac{\partial}{\partial n_p}\left(\frac{1}{r_{pq}}\right)ds_q + \iint_{S_W} \sigma_W(q,t)\frac{\partial}{\partial n_p}\left(\frac{1}{r_{pq}}\right)ds_q = \frac{\partial \phi_0(p,t)}{\partial n_p} \qquad (p \in \Gamma_W). \tag{11}$$

In the desingularized method, the source distribution is outside the fluid domain so that the source points never coincide with the field points (control or collocation points) and therefore the integrals are non-singular. In addition, because of the desingularization, we can use simple isolated Rankine sources and obtain the equivalent accuracy. This greatly reduces the complexity of the form of the influence coefficients that make up the elements of the kernel matrix (Zhang *et al*. 2006). Then the integral equations in Eqs. (10) and (11) can be replaced by a discrete summation of N-isolated singularities located at a small distance away from the corresponding nodal point on the free surface and body

$$\sum_{i=1}^{N} \sigma(q_i,t)\frac{1}{r_{pq_i}} = \phi_0(p,t) \qquad (p \in \Gamma_F) \tag{12}$$

$$\sum_{i=1}^{N} \sigma(q_i,t)\frac{\partial}{\partial n_p}\left(\frac{1}{r_{pq_i}}\right) = \frac{\partial \phi\,(p,t)}{\partial n_p} \qquad (p \in \Gamma_F) \tag{13}$$

The desingularized distance between isolated source point and corresponding nodal point is given by

$$L_d = l_d(D_m)^{\beta} \tag{14}$$

where l_d and β are constants and D_m is a measure of the local mesh size (typically the square root of the local mesh area). The accuracy and convergence of the solutions are sensitive to the choices of l_d and β. Therefore, appropriate l_d and β values need to be determined after numerical test. The recommended values are $l_d = 0.5–1.0$ and $\beta = 0.5$. A detailed study with regard to the performance of DBIEM with the desingularization parameters was reported in Cao *et al*. (1991).

Once the above integral equations using isolated Rankine source are solved at each time step, the fluid velocity in Eq. (3) Eq.w (4) can be calculated from direct derivatives,

$$\boldsymbol{V} = \nabla\phi(p,t) = \sum_{\mathbf{i=1}}^{\boldsymbol{N}} \sigma(q_i,t)\,\nabla\left(\frac{1}{r_{pq_i}}\right) \tag{15}$$

4. Time-stepping integration scheme

In order to obtain the velocity potential and free surface elevation at each time step, the fourth-order predictor-corrector Adams-Bashforth-Moulton scheme (ABM4) and mixed Eulerian-Lagrangian (MEL) method are used. Integrating Eqs. (3) and (4) by ABM4 and MEL is called time marching. Using the total derivative $\delta/\delta t = \partial/\partial t + \vec{\mathrm{v}}\cdot\nabla$, the fully nonlinear free surface conditions can be modified as follows in Lagrangian frame

$$\frac{\delta\phi}{\delta t} = -g\eta - \frac{1}{2}\nabla\phi\,\nabla\phi + \nabla\phi\cdot\vec{\mathrm{v}} \tag{16}$$

$$\frac{\delta\eta}{\delta t} = \frac{\partial\phi}{\partial z} - (\nabla\phi - \vec{\mathrm{v}})\cdot\nabla\eta \tag{17}$$

where $\vec{\mathrm{v}}$ represents the node velocity on the free surface. On the moving node on the free surface with semi-Lagrangian approach, $\vec{\mathrm{v}} = (0, 0, \delta\eta/\delta t)$, the node on the free surface is allowed to move only in the vertical direction. Therefore, the free surface boundary conditions can be further expressed as

$$\frac{\delta\phi}{\delta t} = -g\eta - \frac{1}{2}\nabla\phi\,\nabla\phi + \frac{\partial\phi}{\partial z}\left(\frac{\partial\phi}{\partial z} - \frac{\partial\phi}{\partial x}\frac{\partial\eta}{\partial x} - \frac{\partial\phi}{\partial y}\frac{\partial\eta}{\partial y}\right) \tag{18}$$

$$\frac{\delta\eta}{\delta t} = \frac{\partial\phi}{\partial z} - \frac{\partial\phi}{\partial x}\frac{\partial\eta}{\partial x} - \frac{\partial\phi}{\partial y}\frac{\partial\eta}{\partial y} \tag{19}$$

In the semi-Lagrangian approach, a time-stepping integration procedure must be employed to obtain the values of velocity potential and wave elevation on the instantaneous free surface. After solving the boundary value problem and obtaining the fluid velocity on the free surface at each time step, the free surface boundary conditions can be treated as ordinary differential equations to be marched in time. The general form of the dynamic and kinematic boundary conditions Eqs. (18) and (19) can be rewritten as

$$\frac{\delta\phi}{\delta t} = g(\eta, \phi, t) \tag{20}$$

$$\frac{\delta\eta}{\delta t} = f(\eta, \phi, t) \tag{21}$$

ABM4 scheme (Zhang *et al*. 2006) is selected for integrating Eqs. (20) and (21) with time. It is a fourth-order predictor and corrector method which requires only two evaluations of the functions $g(\eta, \phi, t)$ and $f(\eta, \phi, t)$ at each time step. In the ABM4 scheme, the velocity potential and wave elevation are firstly predicted by Adams-Bashforth method as follows

$$\phi_{t+\Delta t} = \phi_t + \frac{\Delta t}{24}(55g_t - 59g_{t-\Delta t} + 37g_{t-2\Delta t} - 9g_{t-3\Delta t}) \tag{22}$$

$$\eta_{t+\Delta t} = \eta_t + \frac{\Delta t}{24}(55f_t - 59f_{t-\Delta t} + 37f_{t-2\Delta t} - 9f_{t-3\Delta t}) \tag{23}$$

and then these are iteratively corrected by Adams-Moulton algorithm

$$\phi_{t+\Delta t} = \phi_t + \frac{\Delta t}{24}(9g_{t+\Delta t} + 19g_t - 5g_{t-\Delta t} + g_{t-2\Delta t}) \tag{24}$$

$$\eta_{t+\Delta t} = \eta_t + \frac{\Delta t}{24}(9f_{t+\Delta t} + 19f_t - 5f_{t-\Delta t} + f_{t-2\Delta t}) \tag{25}$$

where Δt is the time step.

5. Linearised solution of wave elevation

For the periodic oscillation, i.e., $U=A\omega\sin\omega t$, Wu (1998) gave the linearized analytical solution for wave elevation η

$$\eta = -\frac{1}{g}\sum_{n=1}^{\infty} \dot{B}_n(t)\cos k_n\left(x + \frac{L}{2}\right) \tag{26}$$

where $k_n = n\pi/L$, L is the length of the tank. If only the motion of the tank in x direction will be considered, then

$$B_n = 2\omega_n \omega A \frac{(-1)^n - 1}{k_n^2 L} \frac{\omega_n \sin(\omega t) - \omega \sin(\omega_n t)}{\omega_n^2 - \omega^2} \tag{27}$$

where $\omega_n = \sqrt{gk_n \tanh(k_n h)}$, A is the amplitude of oscillation in x direction, and h is the water depth.

If we further consider the problem with coupled surge and sway motions, i.e., $U_x=A_x\omega_x\sin\omega_x t$ and $U_y=A_y\omega_y\sin\omega_y t$, the 3D linearized analytical solution of free surface elevation can be given as follows

$$\eta = -\frac{1}{g}\sum_{n=1}^{\infty} \dot{B}_{nx}(t)\cos k_{nx}\left(x + \frac{L}{2}\right) - \frac{1}{g}\sum_{n=1}^{\infty} \dot{B}_n(t)\cos k_{ny}\left(y + \frac{B}{2}\right) \tag{28}$$

where B is the breadth of the tank,

$$k_{nx} = n\pi/L, \quad B_{nx} = 2\omega_{nx}\omega_x A_x \frac{(-1)^n - 1}{k_{nx}^2 L} \frac{\omega_{nx}\sin(\omega_x t) - \omega_x \sin(\omega_{nx} t)}{\omega_{nx}^2 - \omega_x^2}$$
$$k_{ny} = n\pi/B, \quad B_{ny} = 2\omega_{ny}\omega_y A_y \frac{(-1)^n - 1}{k_{ny}^2 B} \frac{\omega_{ny}\sin(\omega_y t) - \omega_y \sin(\omega_{ny} t)}{\omega_{ny}^2 - \omega_y^2} \tag{29}$$

and

$$\omega_{nx} = \sqrt{g k_{nx} \tanh(k_{nx} h)}, \quad \omega_{ny} = \sqrt{g k_{ny} \tanh(k_{ny} h)} \tag{30}$$

It should be noted that the natural frequencies in the 3D cases are (Liu and Lin 2008)

$$\omega_{mm}^2 = \sqrt{\left(\frac{mg\pi}{L}\right)^2 + \left(\frac{mg\pi}{B}\right)^2} \tanh \sqrt{\left(\frac{m\pi h}{L}\right)^2 + \left(\frac{m\pi h}{B}\right)^2} \ (m, n = 0, 1, 2, \cdots) \tag{31}$$

6. Numerical results and discussions

We first consider periodic oscillation with

$$U = A\omega \sin\omega t \tag{32}$$

where ω is excitation frequency. In our simulation, the length of tank L is 1m, depth-length ratio h/L=0.5, and breadth-length ratio B/L=0.5. The non-dimensional time $\tau = t\sqrt{h/g}$ is also used.

6.1. Convergence study

Firstly, we studied the effect of l_d in the DBIEM for the 3D sloshing wave. In these cases, the tank is divided in x-direction by $N_x = 21$ intervals, in y-direction by N_y=11 intervals and in z-direction by $N_z = 15$ intervals, as shown in Fig. 2. In order to compare with the linearized analytical solution, the numerical simulation is carried out with small amplitude. In the calculation, we have chosen $\omega = 0.9\omega_1$, $A = 0.001h$ and $\Delta\tau = 0.05$, which have been found to give converged results, where ω_1 is the lowest natural frequency of fluid in the tank due to the motion in the x-direction. The time history of free surface at ($x = -L/2$, $y = 0$) is presented in Fig. 3(a). The conservation of fluid mass has been checked as shown in Fig. 3(b). Comparison between the analytical solution and the numerical results shows that good agreement can be obtained while l_d was chosen between 0.75 and 1.25. We can see that the volume error (while $l_d = 0.5$) is bigger than the other cases. Hereby, we choose l_d as 0.85 in our work.

Fig. 4(a) presents the wave history at ($x = -L/2$, $y = 0$) with four different time intervals and the relative volume error is shown in Fig. 4 (b). In the numerical simulation, the time step should satisfy the Courant condition. It can be seen that good agreement can be obtained when $\Delta\tau$ is less than 0.05.

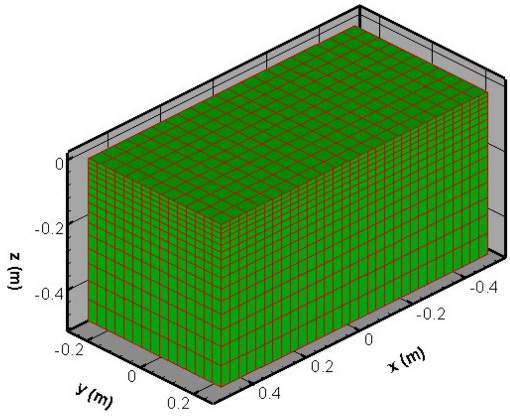

Fig. 2 Mesh for numerical simulation of sloshing wave

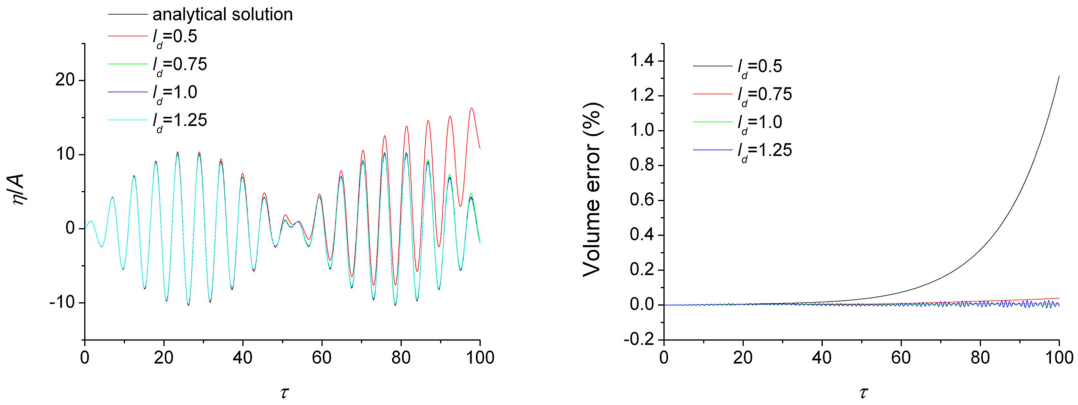

(a) Wave elevation history (b) Relative volume error

Fig. 3 Time history of free surface elevation at ($x = -L/2$, y=0) and relative volume error for different l_d with $\omega = 0.9\omega_1$, $A = 0.001\ h$ and $\Delta\tau = 0.05$

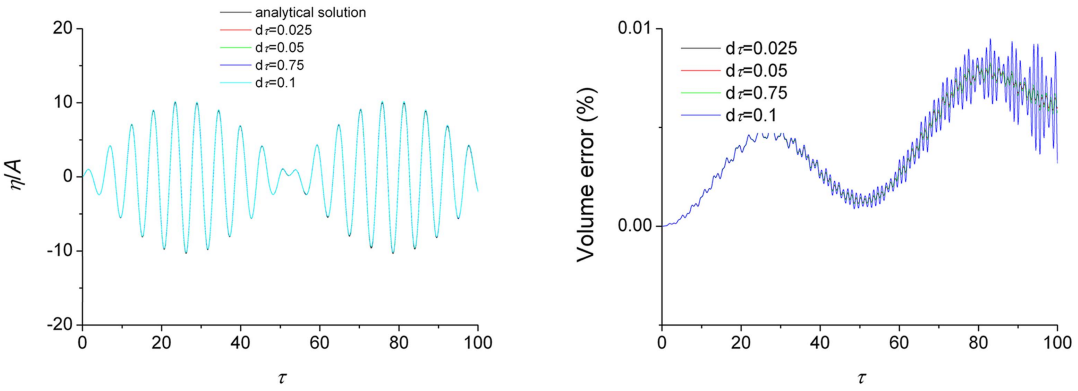

(a) Wave elevation history (b) Relative volume error

Fig. 4 Time history of free surface elevation at ($x = -L/2$, $y = 0$) and relative volume error for different $\Delta\tau$ with ω=0.9ω_1, $A = 0.001h$ and l_d =0.85

6.2. Accuracy check

To further investigate the accuracy of the present simulation, four different excitation frequencies, which are either higher or lower than the first natural frequency in x direction, have been considered. We have chosen $\omega = 0.5\omega_1$, $\omega = 0.9\omega_1$, $\omega = 0.999\omega_1$, $\omega = 1.1\omega_1$, $A = 0.001h$, $\Delta\tau = 0.05$. The time history of free surface elevation at ($x = -L/2$, $y = 0$) is presented in Fig. 5. One can see from Fig. 5(c) that the wave amplitude increases with time as the excitation frequency is very close to the first natural frequency in x direction. Indeed, the magnitude of η/A has reached around 30 at $\tau = 100$. However, it does not suggest that the amplitude will tend to infinity with time in the fully nonlinear simulation. We also can see from Figs. 5(b) and 5(d) that the wave history is very similar to that due to two harmonic wave trains of slightly different frequencies. The details for amplitude modulated wave can be found from Wu *et al*. (1998). It can be suggested that the numerical simulation gives fairly agreement with the linear analytical solution in the limit of the excitation amplitude is small.

6.3. Nonlinear effect at larger amplitude

To demonstrate the effects of the non-linearity, the results for different excitation amplitudes are plotted in Fig. 6, where $\omega = 0.9\omega_1$. It can be observed that with the increase of amplitude A, the

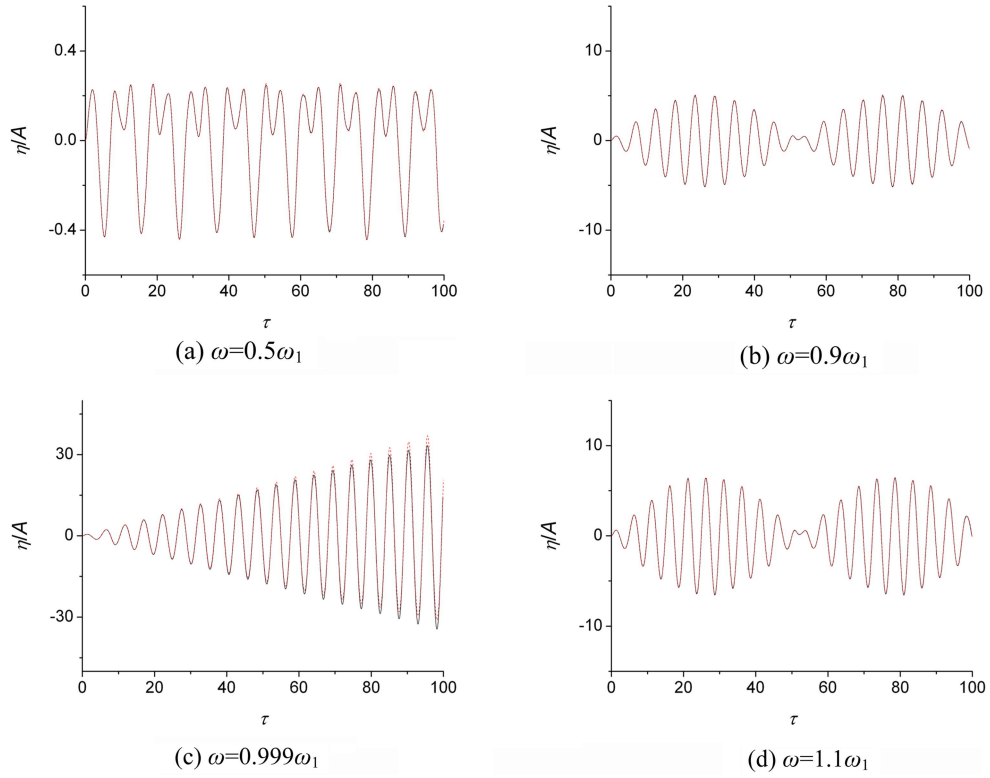

Fig. 5 Comparison of free surface elevation at ($x = -L/2$, $y = 0$) in an excited tank between the present fully nonlinear solution (red dash line) and analytical solution (black line)

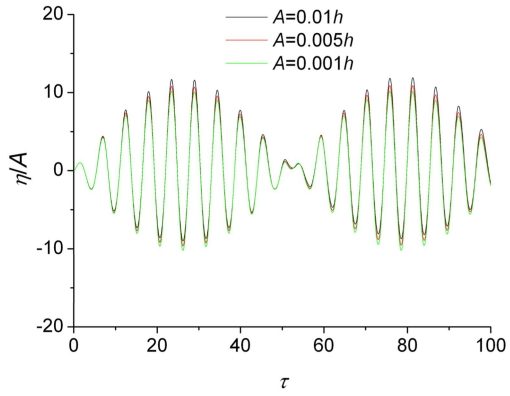

Fig. 6 Wave elevation history at ($x = -L/2$, $y = 0$) for different excitation amplitudes with $\omega = 0.9\omega_1$

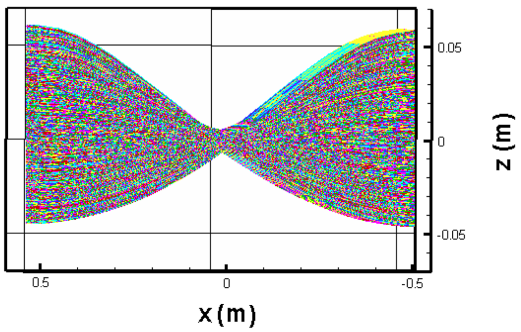

Fig. 7 Wave profiles with $\omega = 0.9\omega_1$ and $A = 0.01\ h$

crests become sharper and the troughs become flatter, as shown in Fig. 6. In our simulation, Fig. 7, which is the wave profile with $\omega = 0.9\omega_1$ and $A = 0.01h$, shows the occurrence of a normal standing wave.

6.4. Simulation of a travelling wave and a bore

We now consider two cases, which were investigated by Wu *et al*. (1998), with $h/L = 0.125$, 0.04, to demonstrate a travelling wave and a bore. In the first case, the tank length is taken as $L = 8$ m. The mesh is generated using $N_x = 41$, $N_y = 5$, $N_z = 16$ and the non-dimensional time step is chosen as $\Delta\tau = 0.0273$. Fig. 8 shows the wave elevation history and wave profile for the amplitude $A = 0.0372h$. Fig. 8(b) clearly exhibits a wave with one peak travelling in the tank. The nonlinear effect is even more significant and the peaks are even sharper here, as shown in Fig. 8(a).

In the second case, the length is taken as $L = 25$ m. The excitation frequency is taken as $\omega = 0.9973\omega_1$ and the amplitude $A = 1.0\ h$. The wave profile is shown in Fig. 9. It can be seen that a bore has occurred at $\tau = 27.5$.

6.5. Irregular excitation for 2D liquid sloshing

We consider the random oscillations of the tank in x direction. For the simulation of the random sloshing, the first thing is to generate a time history of oscillation. As is well known, a random

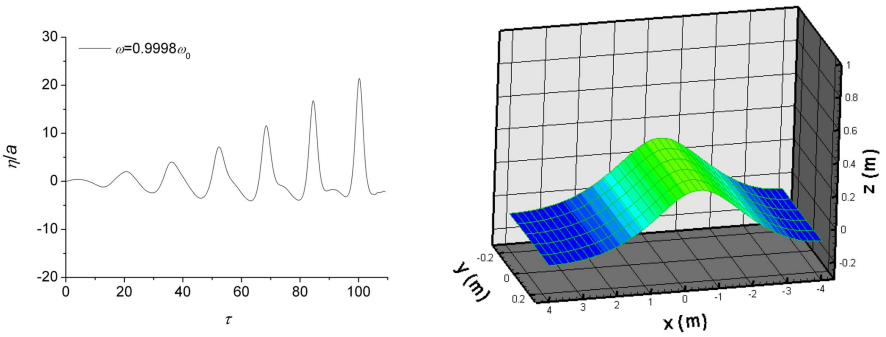

(a) Wave elevation history at (x=-L/2, y=0) (b) Wave profile at τ=103.74

Fig. 8 Wave elevation history and wave profile for h/L = 0.125 and A = 0.0372h

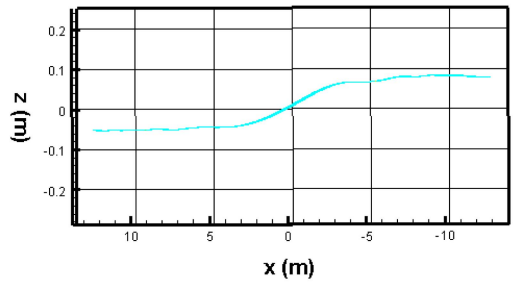

Fig. 9 Wave profile for h/L = 0.04 and A = 1.0 h

wave may be generated using a specified wave spectrum such as Bretschneider spectrum (Wang and Khoo 2005)

$$S_\eta(\omega) = \frac{5H_s^2}{16\omega_p}\left(\frac{\omega_p}{\omega}\right)^5 \exp\left[-\frac{5}{4}\left(\frac{\omega_p}{\omega}\right)^4\right] \tag{33}$$

where H_s is the significant wave height, and ω_p is the peak frequency.

Similar to generate random wave, the motion of the tank can be written as

$$U(t) = \sum_{i=1}^{N_\omega} A_i \omega_i \sin(\omega_i t + \varphi_i) \tag{34}$$

where N_ω is the number of all the linear wave components and φ_i is a random phase angle which uniformly distributed over the range between 0 and 2π. The excitation amplitude A_i is determined by the following equation

$$A_i = \sqrt{2S_\eta(\omega)\Delta\omega} \tag{35}$$

Since higher frequencies have no contribution to generated sloshing wave, we cut-off all the frequencies beyond $5\omega_1$.

Firstly, we consider the irregular excitation with four components illustrated in Table 1. The time

histories of wave elevation at ($x = -L/2$, $y = 0$) and ($x = L/2$, $y = 0$) are shown in Figs. 10(a) and 10(b). The percentage of volume error with time is shown in Fig. 10(c). We can see that the maximum error of the volume is less than 0.02% during the whole simulation. Some snapshots of free surface profiles from $\tau = 87.5$ to $\tau = 100$ with non-dimensional time interval of $\Delta\tau = 2.5$ are shown in Fig. 11. It shows that the wave profiles are a little irregular since the excitation has only with four components which are all close to the lowest natural frequency in x direction.

According to the above computation, it is clear that the present model is effective. Hereby, the random sloshing, based on wave spectrum, will be considered. The specified spectrum of motion with $H_s = 0.005h$ and the peak frequency $\omega_p = \omega_1$ is shown in Fig. 12. In this study, we set $N_\omega = 512$, which is sufficient to describe a random oscillation (Wang and Khoo 2005). The non-dimensional time step $\Delta\tau$ is set to be 0.025. Figs. 13(b) and 13(c) present the wave elevation history at ($x =$

Table 1 Test case for irregular excitation with four components

Index (i)	Excitation frequency ω_i	Amplitude A_i	Phase angle φ_i
1	$0.5\omega_1$	$0.002h$	0
2	$0.9\omega_1$	$0.0002h$	0
3	$1.1\omega_1$	$0.0002h$	0
4	$1.5\omega_1$	$0.002h$	0

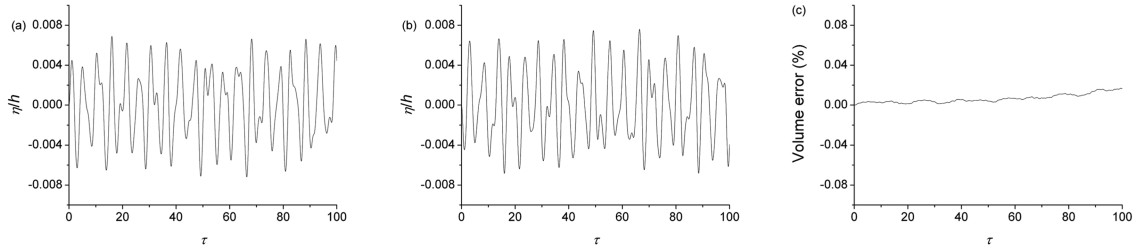

Fig. 10 Wave elevation history and relative volume error (a) ($x = -L/2$, $y = 0$), (b) ($x = L/2$, $y = 0$) and (c) relative volume error

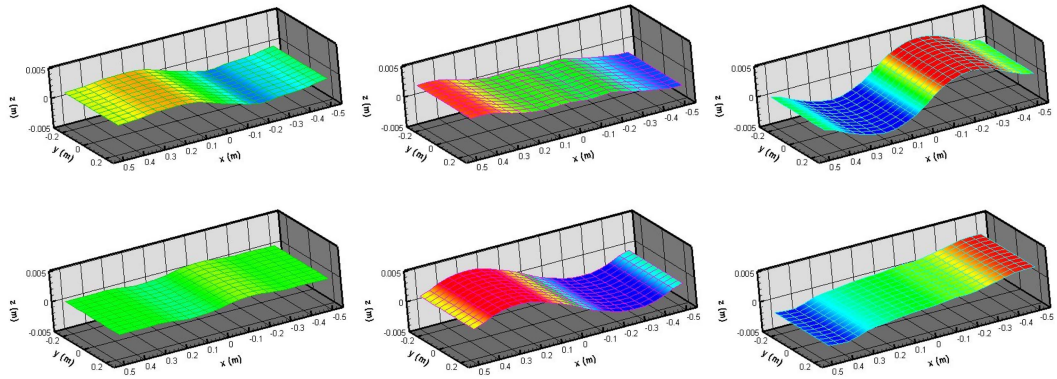

Fig. 11 Free surface profiles between $\tau = 87.5$ and $\tau = 100$ at intervals equal to 2.5

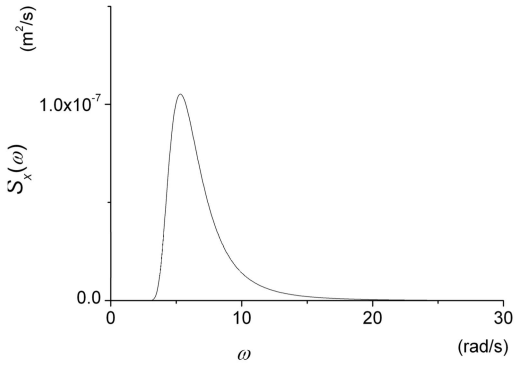

Fig. 12 Spectrum of motion of the tank for $H_s = 0.005\ h$ and $\omega_p = \omega_1$

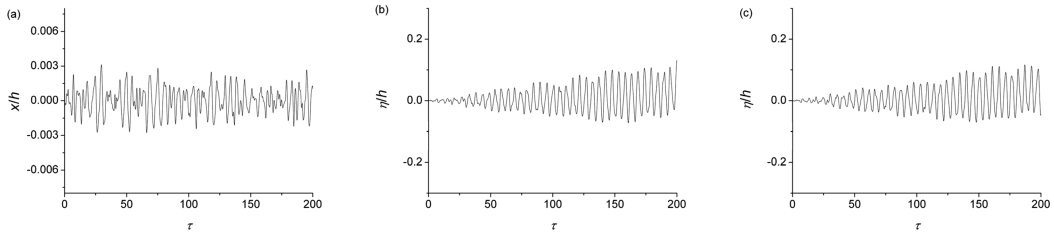

Fig. 13 Horizontal motion and wave elevation history for H_s=0.005h and $\omega_p = \omega_1$ (a) specified oscillation, (b) ($x = -L/2$, $y = 0$) and (c) ($x = L/2$, $y = 0$)

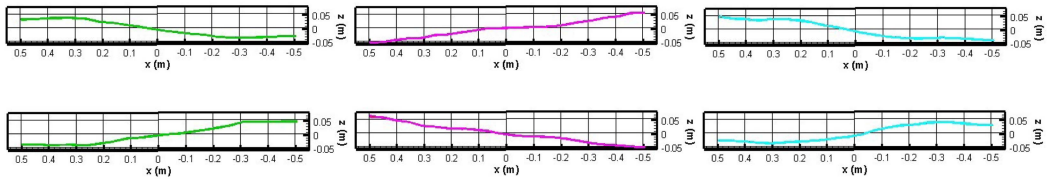

Fig. 14 Free surface profiles between $\tau = 87.5$ and $\tau = 100$ at intervals equal to 2.5 with $H_s = 0.01h$ and $\omega_p = \omega_1$

$-L/2$, $y = 0$) and ($x = L/2$, $y = 0$), respectively. Snapshots of free surface profile are shown in Fig. 14. It is clear that the wave profiles are irregular since the excitation is random.

Since an excitation given to the tank contains many components, the energy of the excitatory spectrum mainly concentrates on some frequencies around the peak frequency, which may vary within a wide range. A resonance of the sloshing wave will occur when the peak frequency is close to the natural frequencies although the resonance is not as violent as that in an excitation of the single frequency. Therefore, a wave spectral investigation based on excitatory spectra with a wide range of peak frequencies is deemed necessary.

Four cases with different peak frequency are considered. For these cases, an identical $H_s = 0.005\ h$ and four different peak frequencies ω_p at ω_1, $0.75\ \omega_1$, $0.5\ \omega_1$ and $0.25\omega_1$ are specified. The spectrums of motion of the tank are presented in Fig. 15. The wave history at ($x = -L/2$, $y = 0$) and ($x = L/2$, $y = 0$) for four different peak frequencies is shown in Fig. 16. We can see that the maximum wave height on the side wall becomes bigger and bigger when the peak frequency is

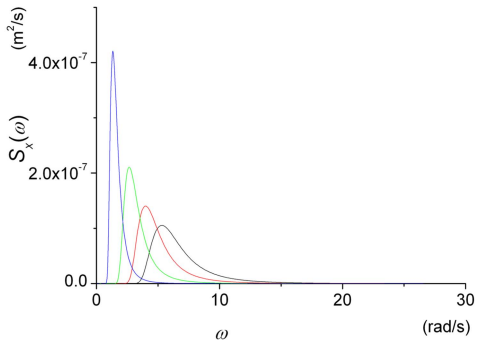

Fig. 15 Spectrum of motion of the tank for H_s=0.005h (black line: ω_p =ω_1, red line: ω_p=0.75ω_1, green line: ω_p= 0.5ω_1 and blue line: ω_p= 0.25ω_1)

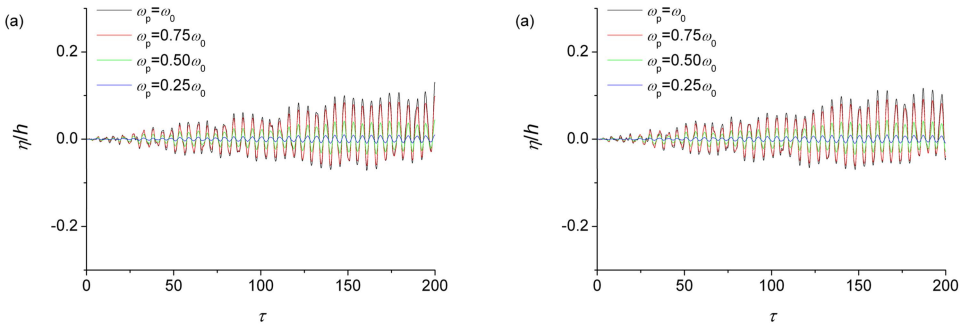

Fig. 16 Wave elevation history for four different peak frequencies with H_s = 0.005h (a) (x = –L/2, y = 0) and (b) (x = L/2, y = 0)

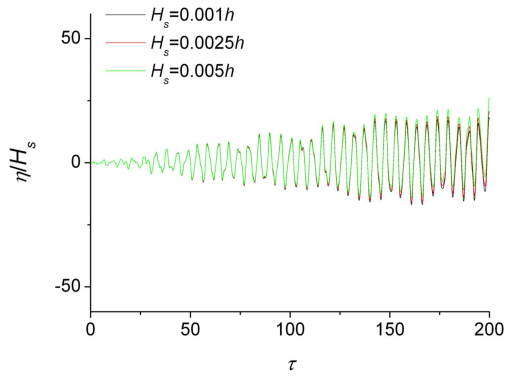

Fig. 17 Wave elevation history at (x = –L/2, y = 0) for different significant wave heights with ω_p = ω_1

close to first natural frequency, even when its peak value of the spectrum of the motion is not large.

Here, we also investigate the nonlinear effect for nonlinear random sloshing wave with same peak frequency ω_p = ω_1. We consider the three cases: H_s = 0.001 h, H_s = 0.0025 h and H_s = 0.005 h. The wave histories are shown in Fig. 17. The figure indicates that the crests and troughs become more and more asymmetrical with the enhancement of nonlinearity of the nonlinear sloshing wave, as also found by Wang and Khoo (2005).

6.6. Irregular excitation for 3D liquid sloshing

In order to investigate the accuracy of the present simulation for three dimensional cases, we first simulate the two cases with regular excitation in both x and y directions: case A (the excitation frequencies are always from lowest natural frequency) with $\omega_x = 0.5\omega_{1x} = 2.658$ rad/s and $\omega_y = 0.5\omega_{1y} = 3.918$ rad/s, and case B (the excitation frequencies are close to lowest natural frequency) with $\omega_x = 0.95\omega_{1x} = 5.051$ rad/s and $\omega_y = 0.95\ \omega_{1y} = 7.445$ rad/s. Here, the lowest natural frequencies of the tank are $\omega_{10} = 5.317$ rad/s and $\omega_{01} = 7.836$ rad/s. The excitation amplitudes of these two cases for both directions are set to 0.001 h. The numerical results of the free surface elevation at the corner of the tank are compared with linearized analytical solution in Fig. 18. Very good agreements are obtained in the comparison.

Based on the above study, then we consider the case with random excitation in both x and y directions. The motions for each direction are based on Eq. (34). We choose $H_{sx} = 0.005\ h$ and $\omega_{px} = \omega_{10}$ for the generation of random excitation in x direction and choose $H_{sy} = 0.005\ h$ and $\omega_{py} = \omega_{01}$ for the generation of random excitation in y direction. We also set $N_\omega = 512$ for both directions and cut-off all the frequencies beyond $5\omega_{1x}$ for the generation of random motion in x direction and cut-off all the frequencies beyond $5\omega_{1y}$ for the generation of random motion in y direction. The numerical results at the four corners of the tank are presented in Fig. 19. It is seen that the wave elevations at four corners are very small for non-dimensional time τ less than 100, then the wave amplitude becomes bigger, gradually. Here, we also investigate the accuracy by checking the conservation of fluid mass, as shown Fig. 20. The maximum volume error is less than 1.5% in the entire simulation. The snapshots of the free surface at $\tau = 187.5$, 190.0, 192.5, 195.0, 197.5 and 200 are shown in Fig. 21, where we can see the irregular 3D free surface obviously.

To investigate the nonlinear effect of sloshing waves under coupled random surge and random sway motion, we consider three cases with $H_{sx} = H_{sy} = 0.001\ h$, $H_{sx} = H_{sy} = 0.0025\ h$ and $H_{sx} = H_{sy} = 0.005\ h$. In these simulations, the peak frequencies of wave spectrum for both directions remain the same as $\omega_{px} = \omega_{10}$ and $\omega_{py} = \omega_{01}$. The wave elevation history at the corner of the tank is shown in Fig. 22. We can see that the nonlinear effect has become much more severe with significant wave height increasing.

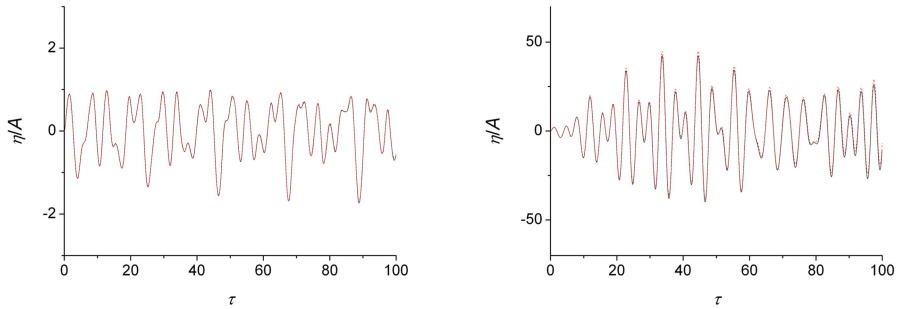

(case A) ω_x=0.5ω_{1x} and ω_y=0.5ω_{1y} (case B) ω_x=0.95ω_{1x} and ω_y=0.95ω_{1y}

Fig. 18 Comparison of free surface elevation at (–L/2, –B/2) in an excited tank between the present fully nonlinear solution (red dash line) and analytical solution (black line)

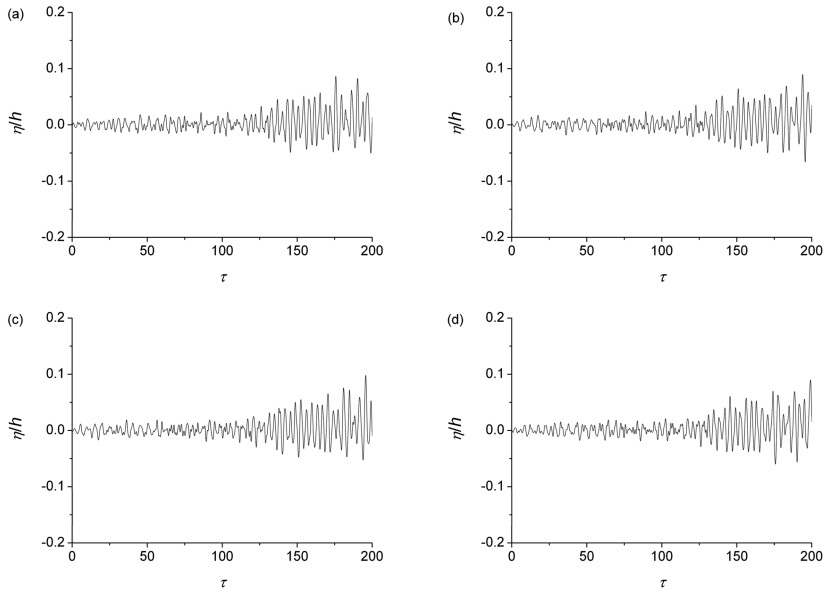

Fig. 19 Wave elevation history at the four corners of the tank undergoing random excitation on both x and y directions (a) ($-L/2$, $-B/2$), (b) ($L/2$, $-B/2$) and (c) ($-L/2$, $B/2$), (d) ($L/2$, $B/2$)

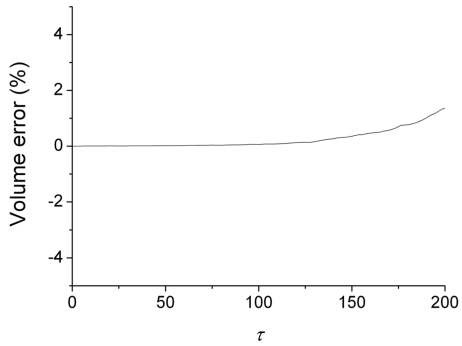

Fig. 20 Relative volume error for $H_{sx} = 0.005\ h$, $\omega_{px} = \omega_{10}$ and $H_{sy} = 0.005\ h$, $\omega_{py} = \omega_{01}$

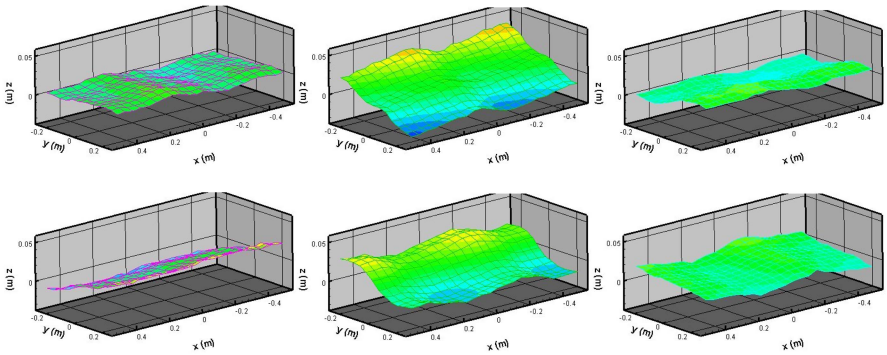

Fig. 21 Free surface profiles between $\tau = 187.5$ and $\tau = 200$ at intervals equal to 2.5 for $H_{sx} = 0.005\ h$, $\omega_{px} = \omega_{10}$ and $H_{sy} = 0.005\ h$, $\omega_{py} = \omega_{01}$

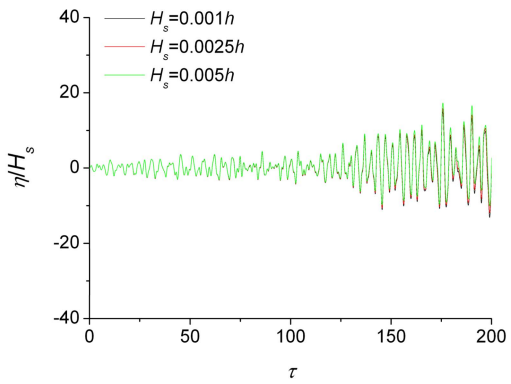

Fig. 22 Wave elevation history at ($-L/2$, $-B/2$) for different significant wave heights with $\omega_{px} = \omega_{10}$ and $\omega_{py} = \omega_{01}$

7. Conclusions

In this paper, DBIEM coupled with MEL time marching scheme is applied to simulate sloshing waves in a 3D tank undergoing specified horizontal motion. The fourth-order predictor–corrector ABM4 scheme is used for the time-stepping integration of the free surface boundary conditions. The position of instantaneous free surface is tracked by applying semi-Lagrangian approach. The saw-tooth instability is overcome by applying B-spline smoothing scheme to both the longitudinal and transverse directions during the simulation. The model is validated by available linear theory and by checking the conversation of fluid mass. All the numerical results agree fairly with the linear analytical solution for small amplitude cases. The sloshing wave due to specified random motion was studied and the typical nonlinear feature of nonlinear waves was captured: steeper peaks and flatter troughs. The wave elevation history on the side wall was studied with different peak frequencies, which was used for generation of the random oscillation. It is found that the maximum wave height on the side wall becomes bigger and bigger when the peak frequency is close to first natural frequency, even if its peak value of the spectrum of the oscillation becomes smaller. It is our interest in future works that the present model be extended to development of 3D sloshing wave in Liquefied Natural Gas Carrier.

Acknowledgments

This paper was made possible by the support of NPRP 08-691-2-289 grant from Qatar National Research Fund (QNRF). The statements made herein are solely the responsibility of the authors.

References

Abramson, H.N. (1996), *The dynamic behavior of liquid in moving containers*, NASA Report, SP 106.
Beck, R.F. (1994), "Time-domain computations for floating bodies", *Appl. Ocean Res*., **16**(5), 267-282.
Cao, Y., Schultz, W.W. and Beck, R.F. (1991), "Three dimensional desingularized boundary integral methods for

potential problems", *Int. J. Numer. Meth. Fl.*, **12**(8), 785-803.
Celebi, M.S. (2001), "Nonlinear transient wave-body interactions in steady uniform currents", *Comput. Method. Appl. M.*, **190**, 5149-5172.
Chen, Bang Fuh and Nokes, R. (2005), "Time-independent finite difference analysis of fully non-linear and viscous fluid sloshing in a rectangular tank", *J. Comput. Phys.*, **209**(1), 47-81.
Cho, J.R. and Lee, H.W. (2004), "Numerical study on liquid sloshing in baffled tank by nonlinear finite element method", *Comput. Method. Appl. M.*, **193**(23-26), 2581-2598.
Faltinsen, O.M. (1978), "A numerical non-linear method of sloshing in tanks with two-dimensional flow", *J. Ship Res.*, **22**, 193-202.
Firouz Abadi, R.D., Ghasemi, M. and Haddadpour, H. (2011), "A modal approach to second-order analysis of sloshing using boundary element method", *Ocean Eng.*, **38**, 11-21.
Frandsen, Jannette B. (2004), "Sloshing motions in excited tanks", *J. Comput. Phys.*, **196**(1), 53-87.
Liu, D.M. and Lin, P.Z. (2008), "A numerical study of three-dimensional liquid sloshing in tanks", *J. Comput. Phys.*, **227**(8), 3921-3939.
Kara, F., Tang, C.H. and Vassalors, D. (2007), "Time domain three-dimensional fully nonlinear computations of steady body-wave interaction problem", *Ocean Eng.*, **34**, 776-789.
Kim, M.H., Celebi, M.S. and Kim, D.J. (1998), "Fully nonlinear interactions of waves with a three-dimensional body in uniform currents", *Appl. Ocean Res.*, **20**, 309-321.
Koo, W.C. and Kim, M.H. (2007), "Fully nonlinear wave-body interactions with surface-piercing bodies", *Ocean Eng.*, **34**(7), 1000-1012.
Solaas, F. and Faltinsen, O.M. (1997), "Combined numerical solution for sloshing in two-dimensional tanks of general shape", *J. Ship Res.*, **41**(2), 118-129.
Sriram, V., Sannasiraj, S.A. and Sundar, V. (2006), "Numerical simulation of 2D sloshing waves due to horizontal and vertical random excitation", *Appl. Ocean Res.*, **28**(1), 19-32.
Wang, C.Z. and Khoo, B.C. (2005), "Finite element analysis of two-dimensional nonlinear sloshing problems in random excitations", *Ocean Eng.*, **32**(2), 107-133.
Wu, Chih Hua and Chen, Bang-Fuh (2009), "Sloshing waves and resonance modes of fluid in a 3D tank by a time-independent finite difference method", *Ocean Eng.*, **36**(6-7), 500-510.
Wu, G.X. (2007), "Second-order resonance of sloshing in a tank", *Ocean Eng.*, **34**(17-18), 2345-2349.
Wu, G.X., Ma, Q.W. and Eatock Taylor, R. (1998), "Numerical simulation of sloshing waves in a 3D tank based on a finite element method", *Appl. Ocean Res.*, **20**(6), 337-355.
Zhang, X.S., Bandyk, P. and Beck, Robert F. (2010), "Seakeeping computations using double-body basis flows", *Appl. Ocean Res.*, 32**(4)**, 471-482.
Zhang, X.T., Khoo, B.C. and Lou, J. (2006), "Wave propagation in a fully nonlinear numerical wave tank: a desingularized method", *Ocean Eng.*, **33**(17-18), 2310-2331.
Zhang, X.T., Khoo, B.C. and Lou, J. (2007), "Application of desingularized approach to water wave propagation over three-dimensional topography", *Ocean Eng.*, **34**(10), 1449-1458.